A New Manufacturing Method for Hourglass Worm Gear Hob Based on a Semi-automatic CAD

LONG Xinjiani[1], *LI Haitao*[1,2*], *RUI Chengjie*[1], *YANG Jie*[1], *ZHANG Xiaodi*[3], *WEI Wenjun*[2]

1. College of Engineering, China Agricultural University, Beijing 100083, P. R. China;
2. Key Laboratory of Optimal Design of Modern Agricultural Equipment in Beijing, China Agricultural University, Beijing 100083, P. R. China;
3. Beijing Kuiente Technology Co., Ltd., Beijing 100043, P. R. China

(Received 27 July 2020; revised 20 October 2020; accepted 20 November 2020)

Abstract: The top relief surfaces of an hourglass worm gear hob are ground manually in the traditional manufacturing process, which cannot ensure the width of the land surfaces of the hob. Moreover, each geometric feature of the hob has been produced through different manufacturing techniques and machine tools, which results in low efficiency. To solve this problem, we propose a semi-automatic computer aided design (CAD) method for hobs. The point clouds of each feature surface of a hob are calculated by combing mathematical equations of the top relief surfaces built by the proposed method with other existing equations of hob surfaces. According to the point clouds, the method can achieve the automatic modeling for the hob in three-dimensional (3D) software by classifying and extracting the parameter information of the feature-hierarchical knowledge of the hob. Based on the generated 3D model, the entire surfaces of the hob can be manufactured on a four-axis computer numerical control (CNC) milling machine through only twice clamping. Verification of the width of the land surface of the hob manufactured by semi-automatic CAD method on a measuring projector proved the precision of the designed width can be ensured. The edge of the contact area on the worm wheel in a meshing experiment is clear and distinct, which means the worm gear drive is meshed well and the hob manufactured by the proposed method has improved machinability. The method simplifies the processing technique, and improves the design efficiency and production accuracy.

Key words: hourglass worm gear hob; top relief surface; feature-hierarchical knowledge; semi-automatic; computer aided design (CAD)

CLC number: TH132.4 **Document code:** A **Article ID:** 1005-1120(2020)06-0914-14

0 Introduction

Hourglass worm drives are extensively used in heavy-loaded and highly-efficiency fields, especially in manufactoring involving iron, steelmaking and hoisting ones[1-2]. Compared with that of cylinder worm gear sets, the lubrication and transmission efficiency of the hourglass worm gear sets are much better[3-5], and they can carry the same load with a more compact volume because of their characteristics, like multi-tooth and double-line contact[6-10]. Therefore, the hourglass worm gear sets can ensure a long service life and a high reliability. However, the mesh theory of the hourglass worm drives is complicated. A precise manufacturing method and a high efficiency manufacturing technique are required because the performances of the drives are sensitive to the manufacturing errors and the assembly errors, and a little error can easily lead to an edge contact[11-12]. The hourglass worm wheel is generally hobbed by a specialized hob that is in accordance

*Corresponding author, E-mail address: h.li@cau.edu.cn.

How to cite this article: LONG Xinjiani, LI Haitao, RUI Chengjie, et al. A new manufacturing method for hourglass worm gear hob based on a semi-automatic CAD[J]. Transactions of Nanjing University of Aeronautics and Astronautics, 2020, 37(6): 914-927.

http://dx.doi.org/10.16356/j.1005-1120.2020.06.009

with the worm. But the hob is difficult to design and manufacture because of its complex geometry features[13].

The traditional production procedures of the hourglass worm gear hob are as follows. First, the original spiral surfaces of the hob are turned or milled from a work blank[14-20]. Second, the spiral surfaces are roughly ground in an hourglass worm-grinding machine. Third, the gashes of the hob are milled and ground and the cutting faces of each cutting tooth can be obtained[21-22]. Fourth, the hob which can be called a semi-finished hob now is quenched to enhance its rigidity[23]. Fifth, each relief surface of the teeth is ground by a grinding wheel manually after the heat-treatment[24]. This process requires different machine tools with different techniques, including a turning or milling machine and a grinding one for rough generating spiral surfaces, a milling machine for rough and fine milling gashes, a grinding machine for fine finishing spiral surfaces[25], a heat-treatment equipment for quenching and a grinding wheel for grinding manual. This leads to a low extent of standardization and a low efficiency in manufacturing[26-27]. Moreover, the manual works and the multiple times of clamping lead to a low precision and consequently a low cutting performance of the hob. Thus, a new production method for hobs is required.

Dong et al. put forward a new design for producing the flank relief surfaces of the hob based on a turning method, in which the flank relief surfaces were turned on a four-axis computer numerical control (CNC) worm turning machine[28-29]. 3D models of some key surfaces of a hob including the flank land surfaces and the flank relief surfaces were established. Moreover, a method on direct-forming of the hob on the four-axis CNC milling machine was preliminary discussed. However, the hob produced by this method still cannot be applied in practice because of the lack of models for some key surfaces of the hob. Liu et al. put forward a flank relief grinding method of a planar double-enveloping worm gear hob by using a four-axis CNC hourglass worm grinding machine[30-31]. In this method, the flank relief surfaces could be ground automatically with a designed land width and an exact relief angle. However, similar to Dong et al.'s method and other existing studies, this method neither provided a model for the top relief surface nor produced a completed physical model of the worm gear hob.

This paper proposes a semi-automatic computer aided design (SA-CAD) method for manufacturing an hourglass worm gear hob. This method can automatically classify and extract the parameter information of the feature-hierarchical knowledge of the hob according to the point clouds of each feature surface, and thus automatically models the hob in 3D software. The point clouds were calculated by the given hob mathematical model. The model is established by combing a presented mathematical equation of the top relief surfaces with other existing equations of hob surfaces. Based on computer aided manufacturing (CAM) technology with the generated 3D model, a milling program for hob milling can be generated. Thus the entire surfaces of the hob can be manufactured on a four-axis CNC milling machine through only twice clamping. The width of the land surfaces can be measured for precision validation. An hourglass worm wheel is hobbed by the hob. Furthermore, a meshing experiment for contact area observation was conducted by installing the worm wheel and the corresponding worm in a gearbox.

1 Features of an Hourglass Worm Gear Hob

The spiral surfaces, the top and root torus of the hob are identical to the parts of the corresponding worm, as shown in Figs.1(a) and (b). For the sake of draining chips, a series of gashes are cut by the cutting faces and the flank faces. In order to hob the worm wheel, a land surface with a certain width that is identical to the spiral surface and top torus must be kept. So the relief surface on every tooth of the hob can prevent interference when hobbing the worm wheel.

The land surface of the teeth can keep the cutting edge of the teeth be used persistently in hob-

bing. The more accurate the width of the land surfaces of the hob, the smoother the hobbing process. A proper width can lessen the vibration of the cutting process and provide a burnishing effect. Fig. 1 (c) shows one of the teeth of the hob. For simplicity, only the right side of the tooth (when viewing from the cutting face side) is discussed. After grinding the flank relief surface and the top relief surface, the spiral surface and the top torus are remained as flank land surface and top land surface, respectively, with a designed width. However, when the grinding depends on manual work, the width cannot be ensured.

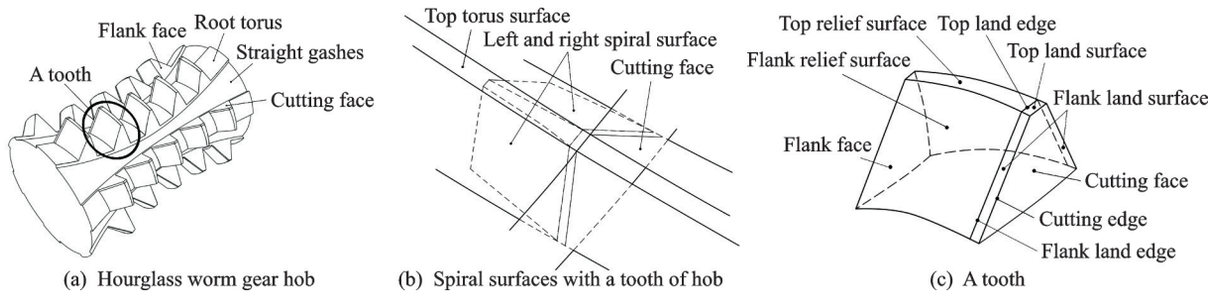

Fig.1 Schematic of an hourglass worm gear hob with straight gashes

2 The Proposed Semi-automatic CAD Method

This section introduces the proposed semi-automatic CAD method for the hourglass worm gear hob. This method deploys the feature hierarchical knowledge classification of the hourglass worm gear hob, the mathematical model of each feature of the hob, the information extraction and automatic 3D modeling algorithm based on the feature-hierarchical knowledge of the hob and the machining process on a four-axis CNC milling machine that only contains two clamping times. Fig. 2 shows the flowchart of the proposed semi-automatic CAD method.

For the purpose of simplifying the whole manufacturing process and improving the accuracy of the features, the first step is to classify the features of the hourglass worm gear hob based on the machining methods and mechanical principles into surfaces based on the structure of the hob. As the surfaces of the hob structure are classified, the mathematical models with key parameters of each surface can be established according to the mechanical principles of the hob machining. In addition, the mathematical model of the top relief surface is built for the first time. The second step is to extract the point data from the mathematical model layer by layer based on the feature-hierarchical knowledge of the hob. In our approach, by using the API functions, an automated modeling algorithm is developed based on the feature-hierarchical knowledge of the hob and point-to-curve-to-surface reverse engineering method. The algorithm can extract the data points from the mathematical model of the hob and automatically deploy the CAD modeling command to model every surface of the hob layer by layer. A milling program is wrote based on the completed 3D model, and the hob is produced on a four-axis milling machine with one rough-milling time and one finish-milling time, only twice.

3 Construction of the CAD Method

3.1 Mathematical model of the hourglass worm gear hob

3.1.1 Coordinate systems

The coordinate systems in Fig.3(a) are all right-handed Cartesian coordinate systems. Fig. 3 (a) illustrates the positional relationship between the hob and the grinding machine in the hob manufacturing process. Subscript "h" represents the hob. Origin O_h is the centre of the hob, stationary coordinate system σ_{oh} (O_{oh}; $\boldsymbol{i}_{oh}$, $\boldsymbol{j}_{oh}$, $\boldsymbol{k}_{oh}$) is connected with

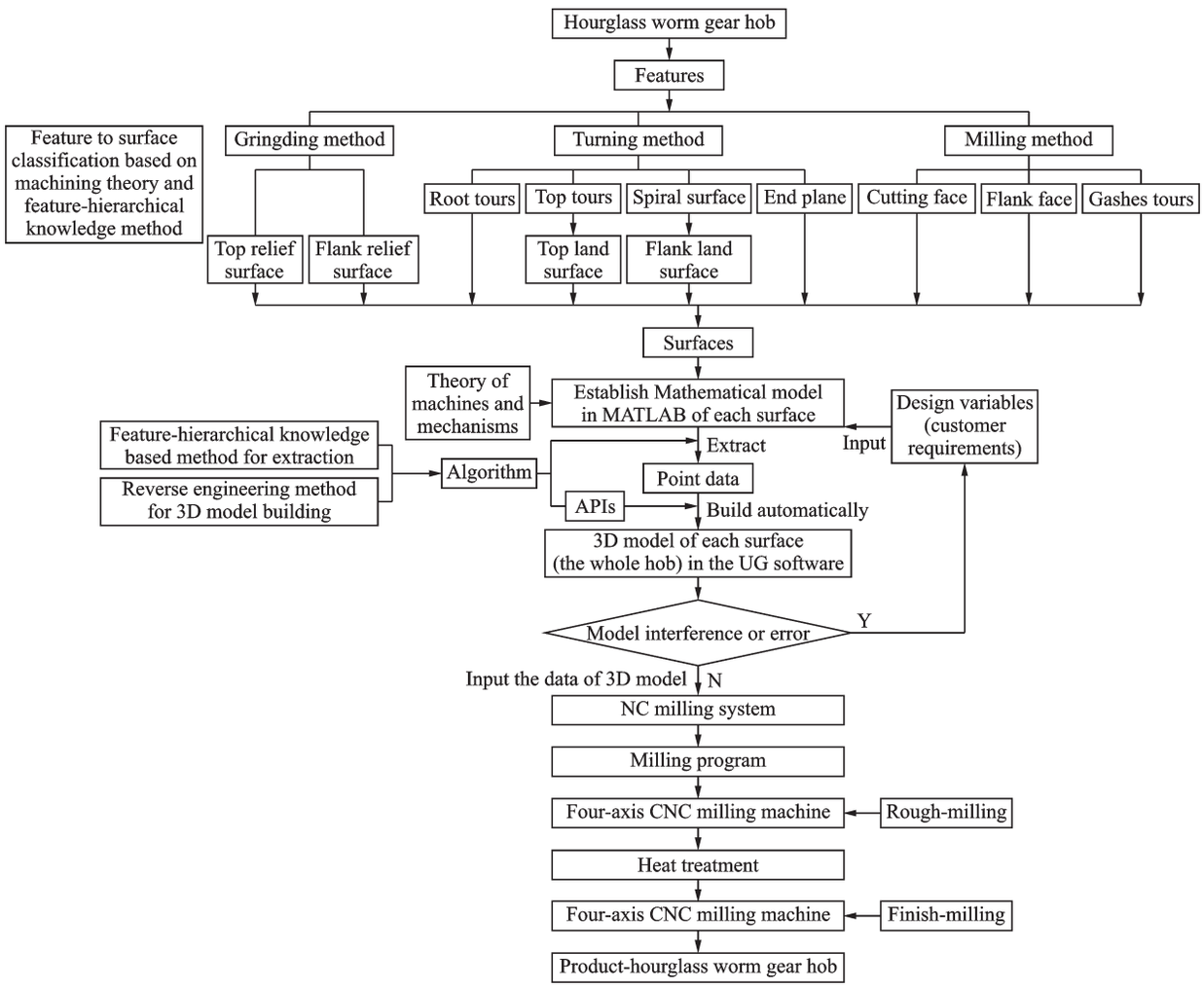

Fig.2 Flowchart of the proposed manufacturing method

the hob. The hob analysed in this paper is right-handed and is rotated around the axis $\boldsymbol{k}_{oh}$ with a rotation angle φ_h when generated. Thus, the moving coordinate system $\sigma_h(O_h;\ \boldsymbol{i}_h,\ \boldsymbol{j}_h,\ \boldsymbol{k}_h)$ is fixed with the hob and $\boldsymbol{k}_h=\boldsymbol{k}_{oh}$. The rotation angle $\varphi_h=0$ and σ_h coincides with σ_{oh} at the start of motion. Subscript "d" represents the grinding machine. Origin O_d is the centre of the grinding machine and is also the centre of the base circle (It is the centre of the worm wheel when O_h is the centre of the worm). Stationary coordinate system σ_{od} $(O_{od};\ \boldsymbol{i}_{od},\ \boldsymbol{j}_{od},\ \boldsymbol{k}_{od})$ is connected with the grinding machine. The grinding machine rotates around the axis $\boldsymbol{k}_{od}$ with a rotation angle φ_d when generating the hob. So the moving coordinate system σ_d $(O_d;\ \boldsymbol{i}_d,\ \boldsymbol{j}_d,\ \boldsymbol{k}_d)$ is fixed with the grinding machine and $\boldsymbol{k}_d=\boldsymbol{k}_{od}$. Axes $\boldsymbol{j}_{od}$ and $\boldsymbol{i}_{od}$ are parallel with axes $\boldsymbol{k}_{oh}$ and $\boldsymbol{i}_{oh}$, respectively. $a=|O_hO_d|$ is the centre distance which represents the vertical distance between the hob axis $\boldsymbol{k}_{oh}$ and the grinding machine axis $\boldsymbol{k}_{od}$.

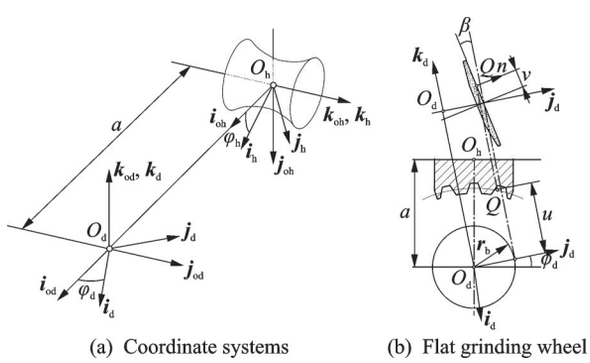

Fig.3 Coordinate systems of the hob and the flat grinding wheel

3.1.2 Mathematical model of the spiral surfaces

The spiral surface of the hourglass worm gear hob, marked as Σ_h, is generated by a plane called generating plane, marked as Σ_d. The generating

plane can be a plane, a single cone or a double cone when rotating around $\boldsymbol{k}_{od}$ at a defined transmission ratio with the hob rotating around $\boldsymbol{k}_{oh}$ at the same time.

Fig.3(b) shows the process that a flat grinding wheel generating the hob. The generating plane is tangent to the main circle of the worm gear with radius r_b. β represents the angle between the rotation axis of the grinding machine and the generating plane. As the parameters of the generating plane, v and u are perpendicular to each other and u is parallel to axis $\boldsymbol{i}_d$. The vector equation of this generating plane in σ_d can be written as

$$(\boldsymbol{r}_d)_d = [-u, r_b - v\sin\beta, v\cos\beta]^T \tag{1}$$

The generated spiral surface Σ_h can be replaced by the generating plane Σ_d using coordinate transformation from coordinate system σ_d to σ_{od}, and then from coordinate system σ_{od} to σ_{oh}, and finally from coordinate system σ_{oh} to σ_h. Point Q in Fig.3 represents the contact point between Σ_d and Σ_h. If $(\boldsymbol{r}_h)_h$ stands for the position vector equation of Σ_h in the moving coordinate system σ_h. The results can be written as

$$(\boldsymbol{r}_h)_h = \boldsymbol{R}[\boldsymbol{k}_h, -\varphi_h] \cdot \{\boldsymbol{R}[\boldsymbol{i}_{oh}, \pi - \varphi_h]\boldsymbol{R}[\boldsymbol{k}_{od}, -\varphi_d](\boldsymbol{r}_d)_d + a\boldsymbol{i}_{oh}\} \tag{2}$$

where

$$\boldsymbol{R}[\boldsymbol{k}_h, -\varphi_h] = \begin{bmatrix} \cos\varphi_h & \sin\varphi_h & 0 \\ -\sin\varphi_h & \cos\varphi_h & 0 \\ 0 & 0 & 1 \end{bmatrix} \tag{3}$$

$$\boldsymbol{R}[\boldsymbol{i}_{oh}, \pi - \varphi_h] = \begin{bmatrix} 1 & 0 & 0 \\ 0 & 0 & -1 \\ 0 & 1 & 0 \end{bmatrix} \tag{4}$$

$$\boldsymbol{R}[\boldsymbol{k}_{od}, -\varphi_d] = \begin{bmatrix} \cos\varphi_d & -\sin\varphi_d & 0 \\ \sin\varphi_d & \cos\varphi_d & 0 \\ 0 & 0 & 1 \end{bmatrix} \tag{5}$$

According to the gearing theory and the generating theory, the spiral surface Σ_h in σ_h can be formulated as

$$\begin{cases} (\boldsymbol{r}_h)_h = [\boldsymbol{r}_h(u_d, v_d, \varphi_d)]_h = [x_h, y_h, z_h]^T \\ \Phi = \Phi_d(u_d, v_d, \varphi_d) = 0 \end{cases} \tag{6}$$

where the first line of Eq.(6) means that the vector of the arbitrary point at the spiral surface Σ_h in coordinate system σ_h; the second line of Eq.(6) is the conjugate condition function. A value of u_d can be calculated from the second line of Eq.(6) when a pair of parameters φ_d and v_d of Σ_d are given; then a point with coordinate (x_h, y_h, z_h) on the spiral surface Σ_h can be found with the first line of Eq.(6) with the value of u_d. An instantaneous contact line can be derived when a value of φ_d and a series values of v_d are given. The spiral surface Σ_h can be calculated as the value of φ_d changes gradually.

3.1.3 Mathematical model of the cutting face and the flank face

The cutting face and the land surface play important roles during a hobbing process as they are impacted by the wheel blank directly. For simplicity, straight gash is selected in this paper. The cutting faces of straight gashes are a series of surfaces passing through the hob rotation axis $\boldsymbol{k}_{oh}$, which is highlighted in red in Fig.4(a). One of these surfaces must go through a point called measuring point of the tooth thickness $\boldsymbol{r}_{SR}$, which can be solved by the

$$\begin{cases} (\boldsymbol{r}_{SR})_h = [\boldsymbol{r}_{SR}(u_{SR}, v_{SR}, \varphi_{SR})]_h = [x_{SR}, y_{SR}, z_{SR}]^T \\ \Phi_d = \Phi_d(u_{SR}, v_{SR}, \varphi_{SR}) = 0 \\ z_{SR} = 0.5S_o \\ (a - \sqrt{x_{SR}^2 + y_{SR}^2})^2 + z_{SR}^2 = (\dfrac{d_F}{2})^2 \end{cases} \tag{7}$$

where d_F means the diameter of the reference torus. The first and the second eqution in Eq.(7) indicate that the measuring point $\boldsymbol{r}_{SR}$ is on the spiral surface.

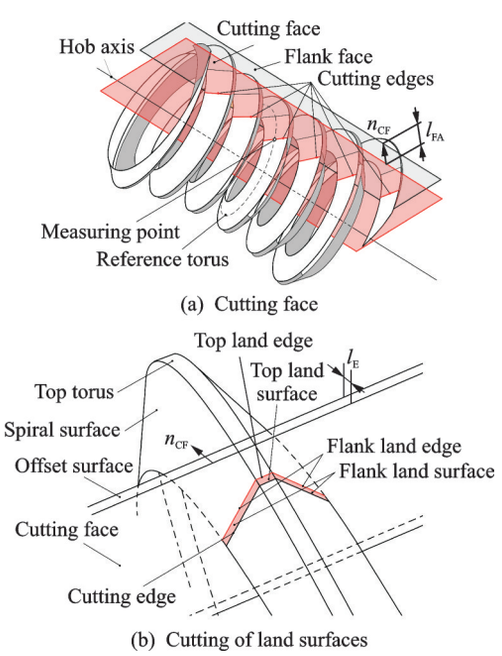

Fig.4 Diagram of the cutting face, the flank face, the land surface, and the land edge

The third and the fourth eqution of Eq.(7) represent the geometric relationship of $\boldsymbol{r}_{SR}$ with the hob model. Specifically, $\boldsymbol{r}_{SR}$ is on the reference torus and it is at a distance between the middle point of the axial tooth thickness S_o to the throat plane.

According to the differential geometry, the expression of the cutting face which passes through the measuring point can be written as

$$\boldsymbol{r}_{CF}(p_{CF},q_{CF})=\left[p_{CF}\frac{x_{SR}}{\sqrt{x_{SR}^2+y_{SR}^2}},p_{CF}\frac{y_{SR}}{\sqrt{x_{SR}^2+y_{SR}^2}},q_{CF}\right]^{T} \tag{8}$$

where subscript "CF" represents the cutting face; p_{CF} stands for the vertical distance between a point on the cutting face to the hob axis; $p_{CF}=0$ when the point is on the hob axis; q_{CF} is perpendicular to p_{CF}.

The other cutting faces can be calculated by rotating Eq.(8) with the hob axis in a designed rotation angle. The cutting edges highlighted in red in Fig.4(a) is defined as the intersection of the cutting face between the spiral surface and the top torus. $\boldsymbol{n}_{CF}$ is a unit normal vector of an arbitrary point on the cutting face. l_{FA} is the width of the tooth. The cutting face can turn to be the flank face by moving along the vector $\boldsymbol{n}_{CF}$ by a distance l_{FA}. Therefore, the equation of the flank face derived from Eq.(8) can be written as

$$\boldsymbol{r}_{FA}(p_{FA},q_{FA})=\left[p_{FA}\frac{x_{SR}}{\sqrt{x_{SR}^2+y_{SR}^2}}-l_{FA}\frac{y_{SR}}{\sqrt{x_{SR}^2+y_{SR}^2}},p_{FA}\frac{y_{SR}}{\sqrt{x_{SR}^2+y_{SR}^2}}+l_{FA}\frac{x_{SR}}{\sqrt{x_{SR}^2+y_{SR}^2}},q_{FA}\right]^{T} \tag{9}$$

where subscript "FA" represents the flank face.

3.1.4 Mathematical model of the land surface

Similar to the establishment of the flank face from the cutting face, an offset surface is built from parallelly moving the cutting face by a distance l_E, which represents the width of the land surface and is highlighted in red in Fig.4(b). Thus, the equation of the offset surface can be formulated as

$$\boldsymbol{r}_{CFF}(p_{CFF},q_{CFF})=\left[p_{CFF}\frac{x_{SR}}{\sqrt{x_{SR}^2+y_{SR}^2}}-l_E\frac{y_{SR}}{\sqrt{x_{SR}^2+y_{SR}^2}},p_{CFF}\frac{y_{SR}}{\sqrt{x_{SR}^2+y_{SR}^2}}+l_E\frac{x_{SR}}{\sqrt{x_{SR}^2+y_{SR}^2}},q_{CFF}\right]^{T} \tag{10}$$

where subscript "CFF" refers to the offset surface. The top torus between the offset surface and the cutting face is then defined as the top land surface; the spiral surface between the offset surface and the cutting face is defined as the flank land surface. The land edges illustrated in red in Fig.4(b) can be defined by the intersection of the cutting face with the spiral surface and the top torus, thus the expression of the flank land edge can be written as

$$\begin{cases}\boldsymbol{r}_{CFF}(p_{CFF},q_{CFF})=[x_{CFF},y_{CFF},z_{CFF}]^{T}\\(\boldsymbol{r}_h)_h=[\boldsymbol{r}_h(u_d,v_d,\varphi_d)]_h=[x_h,y_h,z_h]^{T}\\\Phi=\Phi_d(u_d,v_d,\varphi_d)=0\end{cases} \tag{11}$$

and the top land edge can be formulated as

$$\begin{cases}\boldsymbol{r}_{CFF}(p_{CFF},q_{CFF})=[x_{CFF},y_{CFF},z_{CFF}]^{T}\\(a-\sqrt{x_{CFF}^2+y_{CFF}^2})^2+z_{CFF}^2=\left(\dfrac{d_w^2}{2}\right)^2\end{cases} \tag{12}$$

where d_w is the diameter of the top torus.

3.1.5 Mathematical model of the relief surfaces

As a spatial curved surface, the flank relief surface situated between the flank land edge and the flank face is generated by a type of configuration rules. Dong et al.[29] proposed a generating method where the flank relief surface is generated by a constantly changing transmission ratio modified from the worm meshing ratio during the tool tip turning.

The equation of the flank land edge is evaluated by a given thickness of the flank land surface and a given position of the cutting face. If $E(x_E,y_E,z_E)$ means an arbitrary point on the flank land edge, γ_E means the lead angle of the spiral surface at point E. Based on the given angle of the flank relief surface, the lead angle γ_H of arbitrary point E on the flank land edge can be calculated, and the generating ratio i'_{dh} of the flank relief surface can then be derived. When point E rotates around the grinding machine

axis at an angle φ'_d, with the coordinate transformation from σ_d to σ_{od}, then to σ_{oh}, and finally to σ_h at point E, the equation of the flank relief surface can be formulated in coordinate system σ_h as

$$[\boldsymbol{r}_{CH}(\varphi'_d)]_h=[x_{CH},y_{CH},z_{CH}]^T=$$
$$\boldsymbol{R}\left[\boldsymbol{k}_h,-\frac{\varphi'_d}{i'_{dh}}\right]\cdot$$
$$\left\{\boldsymbol{R}[\boldsymbol{i}_{oh},\varphi_h]\boldsymbol{R}[\boldsymbol{k}_{od},\varphi'_d]_{(r_E)d}+a\cdot\boldsymbol{i}_{oh}\right\} \quad (13)$$

where subscript "CH" stands for the flank relief surface; $(\boldsymbol{r}_E)_d$ the vector $\overrightarrow{O_dE}$ in the coordinate system $\sigma_d(O_d;\ \boldsymbol{i}_d,\ \boldsymbol{j}_d,\ \boldsymbol{k}_d)$; x_H, y_H and z_H mean the coordinate values of a point on the flank relief surface.

3.1.6 Mathematical model of the top relief surfaces

In previous studies in the field, little work has been devoted to the automated method for machining the top relief surface. As the hob is designed for a CNC milling machine, this paper proposes a geometry method instead of a grinding method like the ones proposed by Dong[28] or Liu[30] to build a mathematical model of the top relief surface.

Fig.5(a) is a diagram of the building process. Points A and B are two endpoints of the top land edge, as well as the intersection points of the offset surface, two flank relief surfaces and the top torus. If the coordinates of points A and B are denoted as $A(x_A,y_A,z_A)$ and $B(x_B,y_B,z_B)$, they can be calculated by solving system of Eqs.(14), (15).

$$\begin{cases}\boldsymbol{r}_{CFF}(p_{CFF},q_{CFF})=[x_A,y_A,z_A]^T\\(a-\sqrt{x_A^2+y_A^2})^2+z_A^2=\left(\dfrac{d_w^2}{2}\right)^2\\[\boldsymbol{r}_{CH}(\varphi'_d)]_h=[x_A,y_A,z_A]^T\end{cases} \quad (14)$$

$$\begin{cases}\boldsymbol{r}_{CFF}(p_{CFF},q_{CFF})=[x_B,y_B,z_B]^T\\(a-\sqrt{x_B^2+y_B^2})^2+z_B^2=\left(\dfrac{d_w^2}{2}\right)^2\\[\boldsymbol{r}_{CH}(\varphi'_d)]_h=[x_B,y_B,z_B]^T\end{cases} \quad (15)$$

In order to gain the top relief surface, an auxiliary plane M_o is built. M_o passes along the middle point M of points A and B and is perpendicular to the line $\overline{AB}$. It can be formulated as

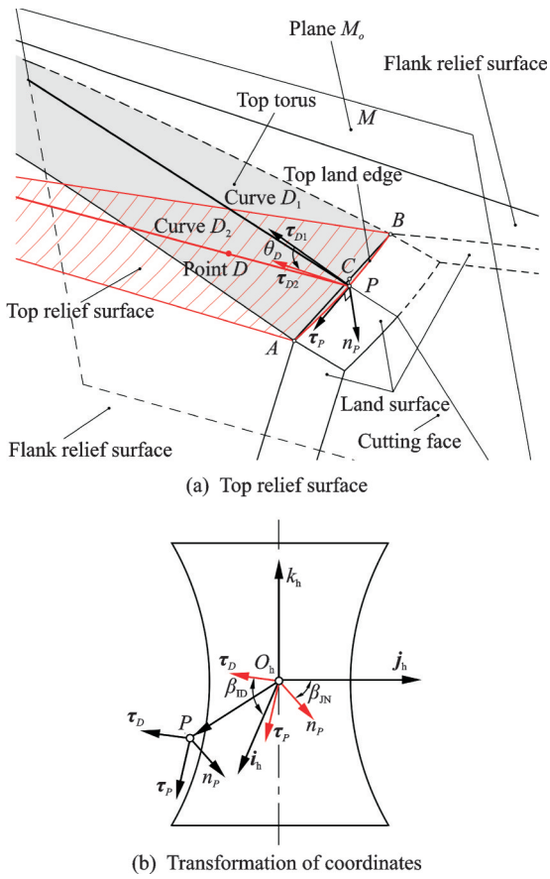

Fig.5 Diagram of top relief surface and relationship between σ_h and σ_P

$$(x_A-x_B)\left(x-\frac{x_A-x_B}{2}\right)+$$
$$(y_A-y_B)\left(y-\frac{y_A+y_B}{2}\right)+$$
$$(z_A-z_B)\left(z-\frac{z_A+z_B}{2}\right)=0 \quad (16)$$

For simplicity, an arbitrary point $M(x_M,y_M,z_M)$ on the plane M_o is used, and the equation of plane M_o in the coordinate system σ_h can be rewritten as

$$(\boldsymbol{r}_M)_h=[x_M,y_M,z_M]^T \quad (17)$$

As the intersection curve of plane M_o and the top torus, curve D_1 can be calculated as

$$\begin{cases}(\boldsymbol{r}_M)_h=[x_{D1},y_{D1},z_{D1}]^T\\(a-\sqrt{x_{D1}^2+y_{D1}^2})^2+z_{D1}^2=\left(\dfrac{d_w^2}{2}\right)^2\end{cases} \quad (18)$$

Point P is the intersection point of plane M_o and the top land edge $\overset{\frown}{AB}$. According to the geometry theory, point P is also the mid-point of $\overset{\frown}{AB}$. It is formulated as

$$\begin{cases} \boldsymbol{r}_{\mathrm{CFF}}(p_{\mathrm{CFF}}, q_{\mathrm{CFF}}) = [x_P, y_P, z_P]^{\mathrm{T}} \\ (a - \sqrt{x_P^2 + y_P^2})^2 + z_P^2 = \left(\dfrac{d_{\mathrm{w}}^2}{2}\right)^2 \\ (\boldsymbol{r}_M)_{\mathrm{h}} = [x_P, y_P, z_P]^{\mathrm{T}} \end{cases} \tag{19}$$

In order to provide a certain angle to the top relief surface, curve D_1 must rotate by a designed top relief angle θ_D around point P into curve D_2 on plane M_o. In another words, $\boldsymbol{\tau}_{D1}$ represents the unit tangent vector of curve D_1 at point P, which is also the unit director normal vector of the top land edge $\widehat{AB}$; $\boldsymbol{\tau}_{D1}$ must rotate a designed top relief angle θ_D around vector $\boldsymbol{\tau}_P$ to become vector $\boldsymbol{\tau}_{D2}$, where $\boldsymbol{\tau}_P$ is the unit tangent vector of the top land edge $\widehat{AB}$ and $\boldsymbol{\tau}_{D2}$ is the unit tangent vector of curve D_2. The process is shown in Fig.5(a). $\boldsymbol{\tau}_{D1}$ can be formulated as

$$(\boldsymbol{\tau}_{D1})_{\mathrm{h}} = (\boldsymbol{n}_P)_{\mathrm{h}} \times (\boldsymbol{\tau}_P)_{\mathrm{h}} \tag{20}$$

where $(\boldsymbol{n}_P)_{\mathrm{h}}$ is the unit normal vector of top torus at point P. According to geometry theory, $(\boldsymbol{n}_P)_{\mathrm{h}}$ is also the unit deputy normal vector of the top land edge $\widehat{AB}$, which can be formulated as

$$(\boldsymbol{n}_P)_{\mathrm{h}} = \left(\frac{\partial F_w}{\partial x_P}, \frac{\partial F_w}{\partial y_P}, \frac{\partial F_w}{\partial z_P}\right) \tag{21}$$

where

$$F_{\mathrm{w}}(x, y, z) = (a - \sqrt{x^2 + y^2})^2 + z^2 - \left(\frac{d_{\mathrm{w}}^2}{2}\right)^2 = 0 \tag{22}$$

As one of the basic trigonal elements of space curve $\widehat{AB}$, $\boldsymbol{\tau}_P$ can be calculated as

$$(\boldsymbol{\tau}_P)_{\mathrm{h}} = (\dot{\boldsymbol{r}}_{AB})_{\mathrm{h}} \tag{23}$$

where $(\boldsymbol{r}_{AB})_{\mathrm{h}}$ is the equation of the top land edge $\widehat{AB}$ in σ_{h}, which has been discussed in 3.1.4.

According to the differential geometry, the three vectors $\boldsymbol{n}_P$, $\boldsymbol{\tau}_P$ and $\boldsymbol{\tau}_{D1}$ can be composed to a coordinate system denoted as σ_P. Fig.5(b) describes the relationship between the coordinate system σ_{h} and σ_P. As the value of these two coordinate systems and point P is known, the angle β_{ID} between axis $\boldsymbol{i}_{\mathrm{h}}$ and vector $\boldsymbol{\tau}_{D1}$ as well as the angle β_{JN} between axis $\boldsymbol{j}_{\mathrm{h}}$ and vector $\boldsymbol{n}_P$ can be calculated. According to coordinate transformation principle, the equation of curve D_2 in coordinate system σ_{h} can be formulated as

$$(\boldsymbol{r}_{D2})_{\mathrm{h}} = \boldsymbol{R}[\tau_{\mathrm{P}}, \theta_D] \cdot \left\{\boldsymbol{R}[\boldsymbol{j}_{\mathrm{h}}, \beta_{\mathrm{ID}}]\, \boldsymbol{R}[\boldsymbol{i}_{\mathrm{h}}, \beta_{\mathrm{JN}}][(\boldsymbol{r}_{D1})_{\mathrm{h}} + \overrightarrow{PO}]\right\} \tag{24}$$

where $(\boldsymbol{r}_{D1})_{\mathrm{h}}$ presents the equation of curve D_1 in coordinate system σ_{h}, as described in Eq.(18); $\boldsymbol{R}[\tau_P, \theta_D]$ the rotation transformation matrices when vector $\boldsymbol{\tau}_{D1}$ rotates around vector $\boldsymbol{\tau}_P$ in angle θ_D, it can be written as

$$\boldsymbol{R}[\tau_P, \theta_D] = \begin{bmatrix} a_1 & a_2 & a_3 \\ b_1 & b_2 & b_3 \\ c_1 & c_2 & c_3 \end{bmatrix} \tag{25}$$

where

$$\begin{cases} a_1 = 1 - (x_\tau^2 + y_\tau^2)(1 - \cos\theta_D) \\ a_2 = x_\tau y_\tau (1 - \cos\theta_D) - z_\tau \sin\theta_D \\ a_3 = x_\tau z_\tau (1 - \cos\theta_D) + y_\tau \sin\theta_D \\ b_1 = y_\tau x_\tau (1 - \cos\theta_D) + z_\tau \sin\theta_D \\ b_2 = 1 - (x_\tau^2 + z_\tau^2)(1 - \cos\theta_D) \\ b_3 = y_\tau z_\tau (1 - \cos\theta_D) - x_\tau \sin\theta_D \\ c_1 = z_\tau x_\tau (1 - \cos\theta_D) - y_\tau \sin\theta_D \\ c_2 = z_\tau y_\tau (1 - \cos\theta_D) + x_\tau \sin\theta_D \\ c_3 = 1 - (x_\tau^2 + y_\tau^2)(1 - \cos\theta_D) \end{cases} \tag{26}$$

when the vector $\boldsymbol{\tau}_P$ is written in $\boldsymbol{\tau}_P(x_\tau, y_\tau, z_\tau)$.

$\boldsymbol{R}[\boldsymbol{j}_{\mathrm{h}}, \beta_{\mathrm{ID}}]$ and $\boldsymbol{R}[\boldsymbol{i}_{\mathrm{h}}, \beta_{\mathrm{JN}}]$ are the rotation transformation matrices from coordinate system σ_{h} to σ_{P}, which is changed with the location of each tooth.

As the equation of curve D_2 is known, denote $D(x_D, y_D, z_D)$ as an arbitrary point on the curve D_2. The top relief surface which is built by the top land edge $\widehat{AB}$ moving parallelly along curve D_2 to form a curved surface $(\boldsymbol{f}_{DP})_{\mathrm{h}}$. It is represented by

$$(\boldsymbol{f}_{DP})_{\mathrm{h}} = (\boldsymbol{r}_{AB})_{\mathrm{h}} + \overrightarrow{PD} \tag{27}$$

where

$$\overrightarrow{PD} = \{x_D - x_P, y_D - y_P, z_D - z_P\} \tag{28}$$

3.2 3D automated modelling of the hourglass worm gear hob

3.2.1 Hob information extraction algorithms

The mathematical model of the hob is built in MATLAB according to section 3.1. The coordinates of points are evenly scattered on each surfaces of the hob and can be calculated. An algorithm is proposed to classify and extract the parameter information of the hob based on the feature-hierarchical

knowledge method. The process is shown in Fig.6.

Firstly, the surfaces are classified into two groups according to the operability of modelling, the regular surface (root surface, gashes tours, end surfaces and top land surfaces) and irregular surfaces (top relief surfaces, flank relief surfaces, flank land surfaces, cutting faces and flank faces). Secondly, the structure-related parameters $\boldsymbol{P}_k$ (denoted as $\boldsymbol{P}_{k1}$, $\boldsymbol{P}_{k2}$, $\cdots$, $\boldsymbol{P}_{kn}$) and the centre distance a, are extracted as values for regular surfaces forming. Since the number of the hob teeth is updated continuously depending on some customer requirements, like the length of the hob, the algorithm has to extract this value for surfaces building subsequently. The irregular surfaces are built based on point-to-curve-to-surface process, so the users have to define the precision of the hob surface modelling, and the precision transfers into the number of points and curves of the surface. Otherwise, the algorithm can use the empirical rules to define them, usually preference as

$$d_{\mathrm{pp}} \leqslant \frac{1}{3} l_{\mathrm{E}} \tag{29}$$

where d_{pp} means the distance between each points.

There are nine types of the irregular surfaces and each type is defined differently. The number of points A_i and curves B_i are defined into the set

$$A_i = \{A_{i1}, A_{i2}, A_{i3}, A_{i4}, A_{i5}, A_{i6}, A_{i7}, A_{i8}, A_{i9}\} \tag{30}$$

$$B_i = \{B_{j1}, B_{j2}, B_{j3}, B_{j4}, B_{j5}, B_{j6}, B_{j7}, B_{j8}, B_{j9}\} \tag{31}$$

And then the sets are distributed to the dynamic array C_{T_m+2} which can be denoted as an ID for each surface.

$$C_{T_m+2}[A_i][B_j] \qquad i = j = 9; m = 7 \tag{32}$$

where m means the number of the teeth surfaces except the top relief surface that equals to 7.

3.2.2 3D automatic modeling algorithms for hob

As the dynamic arrays are defined, the APIs functions based on the reverse engineering method (points-to-curve-to-surface) are programmed to form every surface of the hob automatically. Fig.7 presents the subsection of the automatic modelling of a tooth surface.

3.3 Manufacturing process of the hourglass worm gear hob

Due to the teeth ranging a round the surface of the hob, there needs co-movements including the rotary movement around the hob axis, the rectilinear translation along the hob axis and the radial movement to the hob during the milling process. Therefore, a four- or above-four-axis universal CNC milling machine is recommended. Compared with tradi-

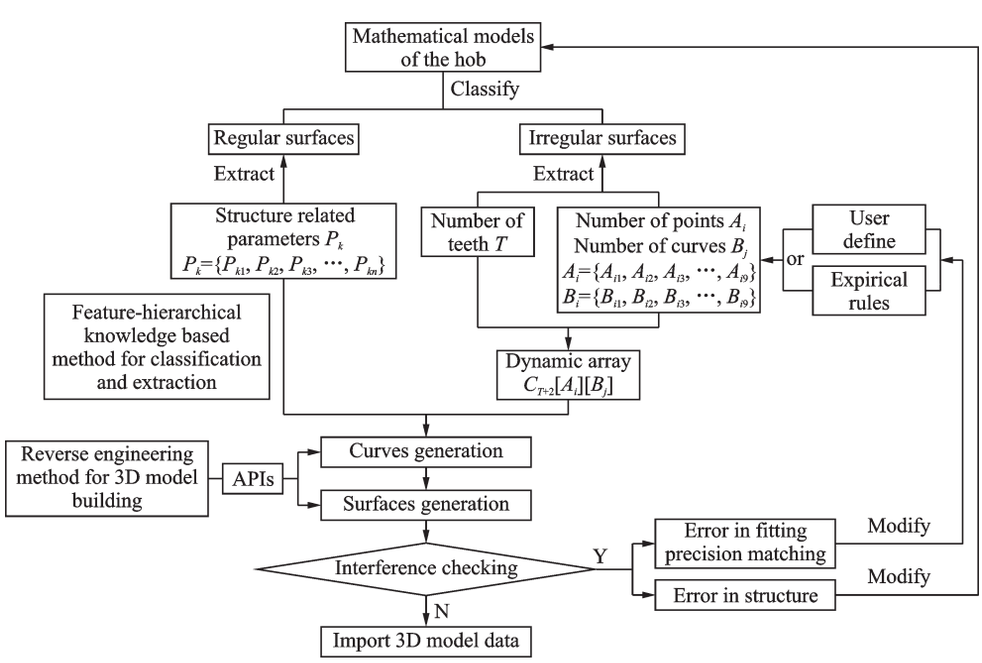

Fig.6 The proposed classification-extraction-modeling algorithm

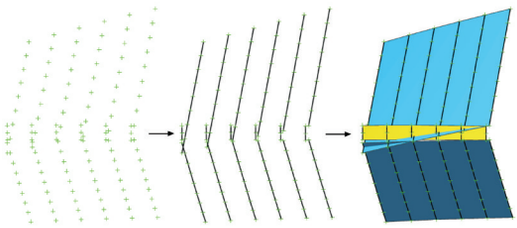

Fig.7 Three-dimensional forming process of a tooth surface

tional manufacturing, the new method experiences less processing and clamping.

This paper suggests the manufacturing on a four-axis universal CNC milling machine. The three processing steps are as follows.

(1) NC rough-milling

Data of the 3D hob model are imported into the CNC system. The hob is clamped into the milling machine by aligning the centre axis, the centre rotation angle and the centre vertical axis of the hob. This is the first time the hob to be clamped. Rough milling the hob is roughly milled and only an allowance is left in the cutting faces and the land surfaces of the teeth for fine finish. In Fig. 8, the red area stands for the remained part for fine finish after rough milling.

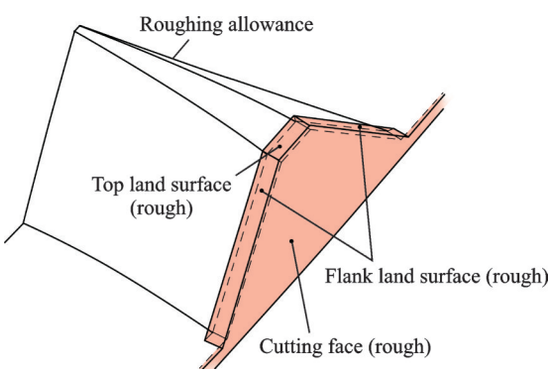

Fig.8 Diagram of remain part of the hob after rough milling

(2) Heat-treatment

In order to improve the solidity, strength and toughness, a heat-treatment, including quenching for the hob after rough milling, is conducted.

(3) NC finish-milling

The hob needs to be fine finish milling as there will be a little surface deformation after the heat-treatment. The allowance on the cutting faces and the land surfaces of the teeth remains as before. This is the second time for the hob to be clamped. The centre axis and the centre rotation axis of the hob are located, as the rough milling process is completed.

4 Experiment

4.1 Design of the hob

This method can be applied to the production of different types of worm gear hobs to achieve higher convenience and accuracy. An hourglass worm gear hob is designed to illustrate this new method. As mentioned in Section 1, it is the cutting edge of the teeth actually plays the role of hobbing the worm wheel. The relief surface of the teeth is used to avoid interference or touching the surface of worm wheel that have just been hobbed. Thus, in the initial design, there is no need to keep the land surface between cutting edge and relief surface, and the existing land surface in the later design is to keep the cutting edge of the teeth be used persistently in hobbing worm wheel. Therefore, the tooth of the hourglass worm gear hob has a characteristic of non-resharpening. In the most design of small size hourglass worm gear hob, the width of the land surface is recommended as 0.1 to 0.2 mm. For the purpose of a better visual effect, the width of the land surface was designed as 1.00 mm in this paper; the angle of the relief surface was designed as 5°. Straight gashes was adopted instead of spiral flutes, as the number of spirals was only 1 and the reference lead angle at gorge of worm was small in this design. The parameters of the hourglass worm gear hob are given in Table 1.

The parameters were substituted into the mathematical model of the hob as represented by Eqs.(1)—(24). The parameter information was extracted and the features of every surface of the hob were built in UG Modelling software automatically. Fig. 9 illustrates the building program and the 3D model of the hob built in UG software. The hourglass worm gear hob was designed to have six straight gashes and 31

Table 1 Main parameters of the worm gearing

Item/unit	Symbols	Value
Number of spirals	z_1	1
Number of teeth of worm wheel	z_2	45
Transverse module of worm wheel/mm	m_t	6.651
Reference pressure angle of worm wheel/(°)	α	23.535 5
Reference lead angle at gorge of worm/(°)	γ_m	7.124 8
Number of teeth enveloping the worm gear	z_k	4.5
Hand of helix		right

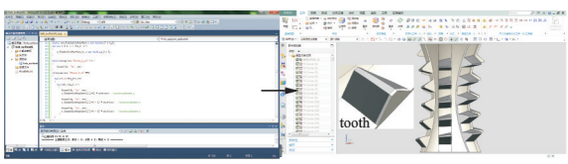

(a) Algorithm process (b) 3D model of the hob

Fig.9 Automatic program and 3D model of the hob in UG software

teeth.

4.2 Hob manufacturing

The hob was manufactured on the model-JD-VT700 four-axis universal CNC machine. The speed of main shaft ranged from 4 000 rad/min to 14 000 rad/min in the rough milling process. The finishing allowance for the cutting faces and the land faces were remained at 0.5 mm thick. The speed of the main shaft remained at 1 000 rad/min in the finish milling step. Fig.10 is a photo of a manufactured hourglass worm gear hob. The land surfaces of the teeth can be seen clearly.

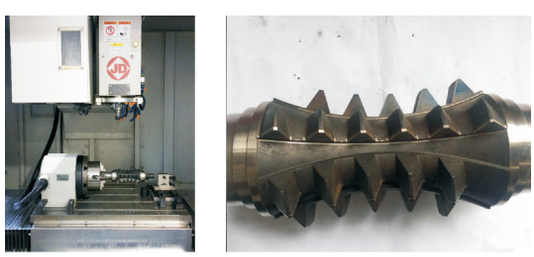

(a) Milling process (b) Hob

Fig.10 The produced hourglass worm gear hob

4.3 Verification of the width of the land surface

4.3.1 Virtual measurement in software

The width of the land surface of the 3D model of the hob was measured in UG. Fig. 11 (a) is a width measurement result of one of the land surfaces, including the top land surface and two flank land surfaces of a tooth. It is seen that the data is very close to the designed width, which means that the 3D hob model has a precise structure corresponding to the mathematical model. The measurement result of the other five arbitrary teeth is shown in Table 2.

4.3.2 Measurement of the finished product

Measurement of the finished product was conducted in a PJ-A3000 Series Measuring Project. Since the hob was designed to be straight gashes, it was placed on the objective table so that the hob axis was vertical to the glass stage. Fig.11(b) shows the placement method and measurement process. As the structure of the hob is special, only one tooth was measured from the top view. The measurement was carried out three times and the result is shown in Table 3.

4.4 Worm gear hobbing

The hob developed by the new method was used to hob the worm wheel on a hobbing machine. Compared with the conventionally-produced one, the hob produced by the new method has advantag-

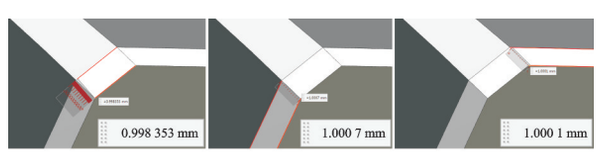

(a) Measurement in software

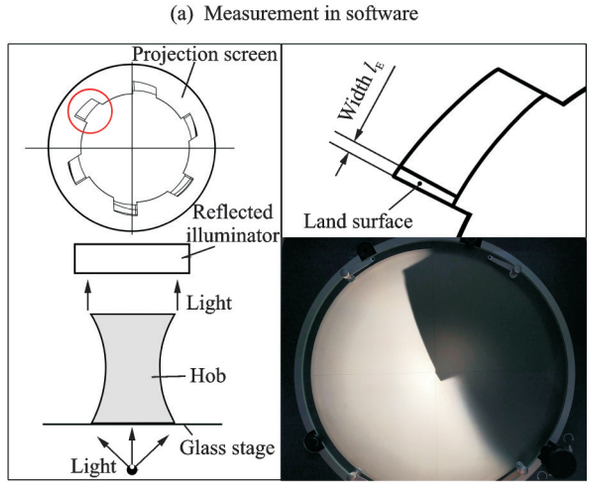

(b) Measurement in projector

Fig.11 Measurements of land surface's width UG and measuring projector

Table 2 Width measurement of land surface of 31 teeth mm

Type	Tooth number					
	1	2	3	4	5	6
Top land surface	0.998 353	0.996 364	1.001 900	0.996 763	0.997 802	0.997 008
Right land surface	1.000 700	1.000 910	0.996 658	0.999 983	1.000 800	1.000 900
Left land surface	1.000 100	0.998 859	0.999 109	1.000 00	0.998 313	0.999 646

Table 3 Width measurement of land surface in the measuring projector

Time	1	2	3	Average
Width/mm	1.034	1.046	1.033	1.037

es of more stable cutting and much less vibration and noise. Fig.12(a) is a detailed view of teeth surface of the worm wheel hobbed by the hob. The surface roughness of the teeth of the worm wheel measured by engineers in the factory was smaller than the conventionally-produced one.

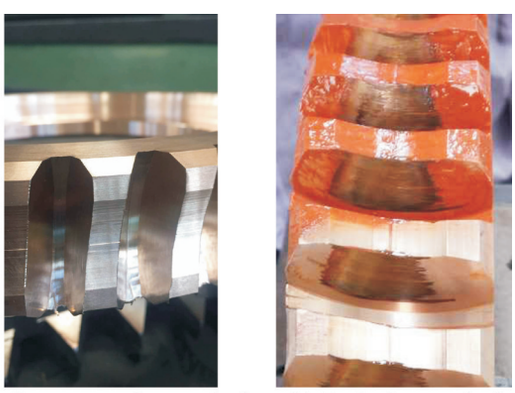

(a) Contact area of worm wheel (b) Teeth of worm wheel

Fig.12 Detailed view of teeth surface of worm wheel and the contact area on the worm wheel teeth after the meshing experiment

4.5 Contact meshing

The worm wheel hobbed by the hob was installed in the gearbox with a corresponding worm. The surfaces of the worm and worm wheel were covered with red lead. Parts of the red lead on the teeth surfaces of the worm wheel were erased and those represent the contact area when the worm pair was meshing. Fig.12(b) shows the contact area on the worm wheel teeth. The edge of the area is clear and distinct, which means the worm gear drive was meshed well and machinability of the hob manufactured by the proposed method has been improved.

5 Conclusions

In order to simplify the processing technique, reduce the design time and improve the production accuracy, we propose a semi-automatic-CAD method for hourglass worm gear hob. The method can achieve the automatic modeling for the hob in a 3D software by classifying and extracting the parameter information of the feature-hierarchical knowledge of the hob, according to the point clouds of each feature surfaces of the hob. These point clouds are calculated by combing a presented mathematical equation of the top relief surfaces with other existing equations of hob surfaces. The hob is then manufactured on a four-axis CNC milling machine using a milling program generated by the 3D model only through twice clamping. The method simplifies the manufacturing technique of the hob.

In addition, the accuracy and efficiency of the manufacturing of the hob is improved. The milling of the land surface can ensure the design width, because the top relief surfaces are modeled by the presented mathematical equations in a 3D software. The edge of the contact area on the worm wheel in meshing experiment is clear and distinct, which demonstrated the worm gear drive is meshed well and the machinability of the hob manufactured by the proposed method has been improved.

References

[1] DONG Xuezhu. Design and modification of enveloping worm gearing[M]. Beijing: China Mechanical Industry Press, 2004. (in Chinese)

[2] ZHOU Liangyong. Modification principle and manufacturing skill of enveloping worm[M]. Changsha: National University of Defense Technology Press, 2005. (in Chinese)

[3] BAO Haoyun, ZHANG Yayun, ZHU Rupeng, et al. Dynamic analysis of external gear system with meshing beyond pitch considering time-varying friction coef-

ficient[J]. Journal of Nanjing University of Aeronautics and Astronautics, 2016, 48(6): 815-821. (in Chinese)

[4] TAKAO S, MINORU M. A study on hourglass worm gearing with developable tooth surfaces[J]. Journal of Mechanical Design, 1978, 100: 451-459.

[5] DONG Xuezhu. Gearing meshing theory[M].Beijing: China Machine Press, 1989. (in Chinese)

[6] WU Xutang. Gear meshing theory[M]. 2nd ed. Xi'an: China Xi'an Jiao Tong University Press, 2009. (in Chinese)

[7] LITVIN F L, FUENTES A. Gear geometry and applied theory[M]. Cambridge, UK: Cambridge University Press, 2004.

[8] SUN Y, GUO Q. Analytical modeling and simulation of the envelope surface in five-axis flank milling with cutter runout[J]. Journal of Manufacturing Science and Engineering—Transactions of the ASME, 2012, 134(2): 021010.

[9] SIMON V. Grinding wheel profile for hob relief grinding[J]. Journal of Mechanical Design, 1982, 104(4): 731-742.

[10] MAITRA G M. Handbook of gear design[M]. India: Tata McGraw-Hill Education, 1994.

[11] SIMON V. Hob for worm gear manufacturing with circular profile[J]. International Journal of Machine Tools & Manufacture, 1993, 33(4): 615-625.

[12] RADZEVICH S P. Dudley's handbook of practical gear design and manufacture[M].2nd ed. Boca Raton, USA: CRC Press, 2012.

[13] RUI C, LI H, YANG J, et al. A design and generating method for grinding relief surfaces of a dual-cone double enveloping hourglass worm gear hob[J]. Journal of Mechanical Design, 2018, 140(12): 123301.

[14] SIMON V. Computer aided manufacturing of high precision hobs[J]. International Journal of Machine Tools & Manufacture, 1988, 28(4): 443-452.

[15] LI Xiaozhen, GAO Qingbin, WANG Rupeng. Dynamic characteristics of modified face-gear drive system[J]. Journal of Nanjing University of Aeronautics and Astronautics, 2016, 48(6): 828-834. (in Chinese)

[16] LI Z M Q, WANG J, ZHU R. Influence predictions of contact effects on mesh stiffness of face gear drives with spur gear[J]. Transactions of Nanjing University of Aeronautics and Astronautics, 2015, 32(5): 566-570.

[17] SIMON V. The influence of hob diameter on worm gear mesh[J]. Symposium on Machine Design, 1985, 4(2): 35-41.

[18] LU H, LIU Z, WANG S. Digitization modeling and CNC machining for enveloping surface parts[J]. International Journal of Advanced Manufacturing Technology, 2014, 73(1/2/3/4): 209-227.

[19] YANG J, LI H, RUI C, et al. Mathematical model and machining method for spiral flute rake faces of hourglass worm gear hob[J]. Transactions of Nanjing University of Aeronautics and Astronautics, 2019, 36(3): 401-412.

[20] LI Haitao, DONG Liyang, SUN Nan, et al. A rough machining method of helical surfaces of enveloping toroidal worm: 200910235344X, China Patent[P]. 2009-10-23. (in Chinese)

[21] YANG J, LI H, RUI C, et al. A method to generate the spiral flutes of an hourglass worm gear hob[J]. Journal of Mechanical Design, 2018, 140(6): 0063301.

[22] YANG Jie, LI Haitao, RUI Chengjie, et al. Design method of spiral flutes rake face of an hourglass worm gear hob[J]. Journal of Beijing University of Aeronautics and Astronautics, 2018, 44(9): 1878-1887. (in Chinese)

[23] LI Haitao, LIU Guanyi, WEI Wenjun, et al. Numerical control grinding method of planar quadratic enveloping worm hob hob angle: 2014106130615, China Patent[P]. 2014-10-06. (in Chinese)

[24] LI Haitao. Research on meshing theory and manufacturing technology of enveloping worm gearing generated by two degree-of-freedom linear cutter edge[D]. Beijing: China Agricultural University, 2009. (in Chinese)

[25] LI H, WEI W, DONG X. Mesh analysis and test verification on two degree of freedom linear cutting tools enveloping worm gears[J]. Journal of Mechanical Engineering, 2011(5): 23-29.

[26] LIU Z, LU H, YU G, et al. A novel CNC machining method for enveloping surface[J]. International Journal of Advanced Manufacturing Technology, 2015, 85(1/2/3/4): 779-790.

[27] LU H, LIU Z, WANG S, et al. Digitization modeling and CNC machining for enveloping surface parts[J]. The International Journal of Advanced Manufacturing Technology, 2014, 73(1): 209-227.

[28] DONG Liyang. Study on NC machining technologies of toroidal worm wheel hob[D]. Beijing: China Agricultural University, 2013. (in Chinese)

[29] DONG L, WANG J, LIU P, et al. An NC rough

turning method of an enveloping toroidal worm[J]. Production Engineering, 2012, 6(2): 129-135.

[30] LIU Guanyi. Research on CNC relief grinding technology of enveloping worm gear hob[D]. Beijing: China Agricultural University, 2016. (in Chinese)

[31] LIU G, WEI W, DONG X, et al. Relief grinding of planar double-enveloping worm gear hob using a four-axis CNC grinding machine[J]. The International Journal of Advanced Manufacturing Technology, 2017, 89(9): 3631-3640.

Acknowledgements This work was supported by The Development of Design and Manufacturing Technology of Double-Enveloping Worm Pair in High-precision with Little Centre Distance (No. 69190135). We would like to thank the Professor Workstation of China Agricultural University in Hebei Baoding Laibo Transmission Machinery Manufacturing Co. LTD (No.20200901).

Authors Ms. **LONG Xinjiani** received her B. S. degree in China Agricultural University in 2016. She is currently a doctoral student in China Agricultural University. Her research interest is focused on rapid, automatic and intelligent design of mechanical products, including the rapid design of hourglass worm gear drive.

Dr. **LI Haitao** received his Ph. D. degree from China Agricultural University, Beijing, China, in 2009. From August 1989, he has been working at China Agricultural University, Beijing. From October 2010, he has been working as a visiting scholar in the Brunel University in the United Kingdom AMEE, engaged in super-precision manufacturing. In May 2015, he joined the Key Laboratory of Optimal Design of Modern Agricultural Equipment in Beijing, China Agricultural University, Beijing.

Author contributions Ms. **LONG Xinjiani** designed the method, established the mathematical model of top relief surfaces, designed the algorithm for information extraction and automatic modeling, interpreted the results and wrote the manuscript. Dr. **LI Haitao** guided the process, and established the mathematical model of other hob surfaces. Mr. **RUI Chengjie** and Mr. **YANG Jie** contributed to the building of the mathematical model of the hob. Ms. **ZHANG Xiaodi** provided the data and experiments. Prof. **WEI Wenjun** contributed to the discussion and background of the study. All authors commented on the manuscript draft and approved the submission.

Competing interests The authors declare no competing interests.

(Production Editor: ZHANG Bei)

一种基于半自动CAD的环面蜗轮滚刀制造方法

龙新佳妮[1]，李海涛[1,2]，芮成杰[1]，杨　杰[1]，张筱迪[3]，魏文军[2]

(1.中国农业大学工学院,北京 100083,中国;
2.中国农业大学现代农装优化设计北京市重点实验室,北京 100083,中国;
3.北京奎恩特科技有限公司, 北京 100043,中国)

摘要:在传统的制造工艺中,环面蜗轮滚刀刀齿的顶后角面由手工磨削,不能保证滚刀刀齿刃带面的宽度;滚刀的每一个几何特征曲面是通过不同的制造工艺采用不同的机床加工生成,工艺繁琐且制造效率低。为了简化滚刀制造工艺,提高制造效率和刃带面的制造精度,本文提出一种滚刀半自动计算机辅助设计(Computer aided design, CAD)方法。首先建立滚刀螺旋面和侧后角面数学模型,在此基础上提出一种滚刀刀齿顶后角面数学模型的建立方法;根据得到的滚刀数学模型计算得到滚刀各特征曲面点云坐标。以点云坐标为基础,通过对滚刀特征层次知识的参数信息进行分类和提取,实现滚刀在三维软件中的自动化建模。根据生成的三维模型,在四轴数控铣床上仅经过两次装夹可加工出完整环面蜗轮滚刀成品。在测量投影仪上对半自动CAD方法制造出的滚刀刀齿刃带面宽度进行测量,证明了刃带设计宽度的精度可以得到保证。在该滚刀滚切出的蜗轮和对应的蜗杆啮合试验中,蜗轮接触区边缘清晰且界限分明,说明了该蜗杆副传动啮合效果良好,用半自动CAD方法制造的滚刀切削性能良好。所提出的半自动CAD方法简化了滚刀制造工艺,提高了滚刀设计效率和制造精度。

关键词:环面蜗轮滚刀;顶后角面;特征层次知识;半自动;计算机辅助设计